

Improved Temperature Dynamic Model of Turbine Subcomponents for Facilitation of Generalized Tip Clearance Control

Javier A. Kypuros, Ph.D., Rodrigo Colson, and Alfredo Muñoz
University of Texas-Pan American, Edinburg, Texas

Abstract

This paper describes efforts conducted to improve dynamic temperature estimations of a turbine tip clearance system to facilitate design of a generalized tip clearance controller. This work builds upon research previously conducted and presented in [1] and focuses primarily on improving dynamic temperature estimations of the primary components affecting tip clearance (i.e. the rotor, blades, and casing/shroud). The temperature profiles estimated by the previous model iteration, specifically for the rotor and blades, were found to be inaccurate and, more importantly, insufficient to facilitate controller design. Some assumptions made to facilitate the previous results were not valid, and thus improvements are presented here to better match the physical reality. As will be shown, the improved temperature sub-models, match a commercially validated model and are sufficiently simplified to aid in controller design.

Nomenclature

<u>Symbol</u>	<u>Units</u>	<u>Description</u>
A	m^2	surface area
V	m^3	volume
L	m	characteristic length ($L = V / A$)
T	$^{\circ}C$	temperature
θ	$^{\circ}C$	temperature differential ($\theta = \Delta T = T(x, t) - T(x, t = 0) = T - T_i$)
c	$J/kg-^{\circ}C$	specific heat
h	$W/m^2-^{\circ}C$	convection heat transfer coefficient
k	$W/m-^{\circ}C$	thermal conductivity
r	m	radius
t	sec	time
w	m	width
α	m^2/sec	thermal diffusivity ($\alpha = k / \rho c$)
δ		penetration depth of surface thermal effects
ρ	kg/m^3	density
ν		Poisson's ratio
η		film cooling effectiveness

1 Introduction

The focus of this study is to improve estimations of the temperature distributions in the rotor, blades, and casing/shroud substructure. Results from the previous model were compared to a validated commercial model. Temperature estimations for the rotor and blades were found to be erroneous, and the casing/shroud substructure was modeled differently. Since the intent of this model is to sufficiently estimate dynamic turbine tip clearance to facilitate controller design, temperature estimations need to be improved while maintaining a relatively simple model. The major culprits responsible for errors are suspected to be a few of the assumptions used to assist in deriving the previous analytical solutions.

The commonly-used semi-infinite solution to the conduction equation with convective boundary condition was previously employed to estimate the surface temperature of the rotor, blades, and shroud:

$$\frac{T_w - T_i}{T_\infty - T_i} = 1 - \exp\left[-\frac{h^2}{\rho c k} t\right] \operatorname{erfc}\left[\sqrt{\frac{h^2}{\rho c k} t}\right] \quad (1)$$

where $T_w = T(x = 0, t)$, $T_i = T(x, t = 0)$, and T_∞ are the surface, initial, and fluid temperatures. This solution was derived making the following assumptions:

1. the heat flows primarily one-dimensionally,
2. the surface is exposed to convection,
3. the temperature of the convective fluid is constant,
4. the average temperature of the component is approximately equal to the surface temperature, and
5. the material properties are assumed to be constant.

The first two assumptions are reasonable but the remaining three are questionable. The temperatures of the fluids flowing over respective surfaces vary with time and that must be accounted for. Some of the components are sufficiently massive that their thermal inertia must be considered. The temperatures vary over significant ranges suggesting that the material property temperature-dependencies may need to be considered. These assumptions are critically evaluated to improve temperature estimations.

Additionally, the steady-state conduction equation applied in the radial dimension was used to determine the temperature distribution through the shroud so that the thermal stress could be calculated,

$$T(r) = T_{s,inner} + (T_{s,outer} - T_{s,inner}) \frac{\ln(r/r_{inner})}{\ln(r_{outer}/r_{inner})} \quad (2)$$

where $T_{s,inner}$ and $T_{s,outer}$ are the inner and outer surface temperatures, respectively. To facilitate this solution, the heat transfer through the shroud was assumed to be quasi-steady-state (i.e. the heat transfer in the shroud was assumed to occur relatively rapidly). As mentioned above, the inner and outer surface temperatures were calculated using the semi-infinite solution. Thus, the same questionable assumptions apply. Furthermore, the quasi-steady-state assumption was never fully validated.

In the subsequent sections, alternative formulations are employed to improve estimation of the temperature distributions. The three major methods used to garner analytical solutions to the transient conduction equation are the lumped-capacitance method, the Laplace transform method, and the approximate method of assumed solutions. The remainder of this document describes the resulting solutions and shows which methods provided the best estimations for each of the components.

2 Improved Temperature Estimation

The methods employed here to derive analytical solutions are intended to critically evaluate the validity of the questionable assumptions detailed above. The rotor is first evaluated and alternative solutions that incorporate transient boundary conditions are derived. As will be shown, the transient boundary conditions are more important in approximating the average temperature of the rotor than the temperature-dependent material properties. Further investigation of the turbine blades suggested that the relatively low ratio of volume to surface area of the blades would facilitate use of the lumped-capacity method. Results detailed below will show that the average blade temperature can be reasonably approximated by assuming constant material properties and incorporating the transient boundary condition into the lumped-capacity method. The casing/shroud substructure is the least investigated in the literature so a formulation similar to that suggested for the rotor is detailed below. However, at this time there are no readily available validated results to confirm the accuracy or appraise estimation improvement due to this formulation.

2.1 Rotor

As previously mentioned, the rotor temperature was originally calculated using Equation (1). Equation (1) was derived using the Laplace transform method and assumes that the convective surface is exposed to a fluid at a constant temperature. Additionally, the average temperature was assumed to be approximately equal to the surface temperature. To better calculate average rotor temperatures, the temperature distribution should be integrated with respect to x (the distance measured from the surface across the width of the solid) and divided by the rotor width, w ,

$$\theta_{average} = \frac{1}{w} \int_0^l \theta(x,t) dx. \tag{3}$$

By applying Laplace transforms¹, to the 1-D conduction equation,

$$\frac{\partial \theta}{\partial t} = \alpha \frac{\partial^2 \theta}{\partial x^2}, \tag{4}$$

it can be shown that the temperature distribution in a semi-infinite solid is

$$\theta(x,t) = \frac{h}{k} \left[\sqrt{\frac{\alpha}{\pi t}} \exp\left(\frac{-x^2}{4\alpha t}\right) - \frac{h}{k} \alpha \exp\left(\frac{h}{k} x + \left(\frac{h}{k}\right)^2 \alpha^2 t\right) \operatorname{erfc}\left(\frac{x}{\sqrt{4\alpha t}} + \frac{h}{k} \sqrt{\alpha t}\right) \right] * \theta_{\infty}(t). \tag{5}$$

where $\theta_{\infty} = T_{\infty} - T_i$. Note that for a constant fluid temperature (i.e. $\theta_{\infty} = \text{constant}$) the above solution evaluated at the surface ($x = 0$) simplifies to Equation (1). The presence of a convolution (*) and the multiplication of an exponential and error function make this equation difficult to integrate analytically with respect to x to calculate the average temperature. Moreover, as shown in Figure 1, the rotor does not have only a single surface exposed to convection as is assumed for a semi-infinite solid but two surfaces.

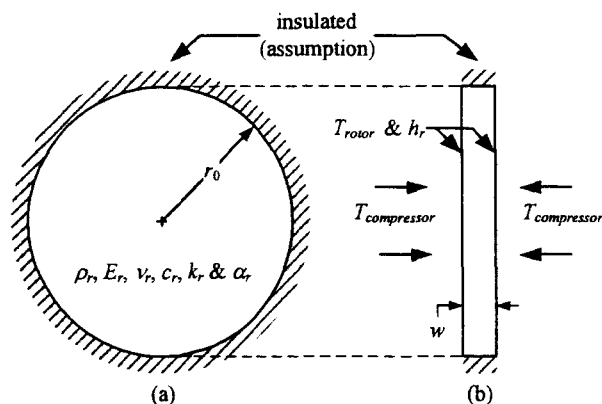


Figure 1. Rotor schematic: (a) frontal view and (b) cross-sectional view.

To facilitate a simpler, closed-form approximation that can accommodate the two convection boundary conditions, the method of assumed solutions is employed. This approximate method as detailed in [2] utilizes the integral form of the conduction equation and an assumed temperature profile (usually defined as a polynomial which is easily integrated) that matches the boundary and initial conditions. The integral form of the conduction equation is [4,5]

¹ Refer to [2,3] for use of the Laplace transform in solving the 1-D conduction equation. These references also include useful transform tables.

$$\frac{d}{dt} \left[\int_0^{\delta} \theta(x,t) dx \right] - \theta(\delta,t) \frac{\partial \delta}{\partial t} = \alpha \left[\frac{\partial \theta}{\partial x} \Big|_{x=\delta} - \frac{\partial \theta}{\partial x} \Big|_{x=0} \right] \quad (6)$$

where δ is the penetration depth shown in

Figure 2. It is the depth from the surface to which the thermal effects are felt (i.e. the distance from the surface where the temperature gradient goes to zero).

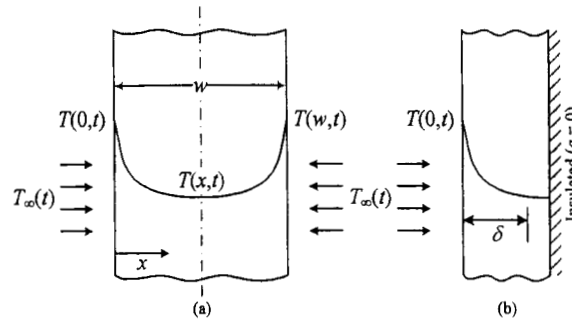


Figure 2. (a) Infinite slab temperature distribution and (b) insulated centerline assumption.

As shown in Figure 3, as $t \rightarrow \infty$ the thermal effect of the convection fully penetrates (i.e. $\delta = w/2$) at which point the temperature profile is fully developed and begins to move up the temperature axis. After this, the penetration depth remains constant. Prior to this instant the temperature change at the centerline remains zero. Hence, to properly capture the temperature profile, the solution must be broken into two parts: (1) for $\delta < w/2$ and (2) for $\delta = w/2$. Moreover, while $\delta < w/2$, the temperature profile only applies to the interval $0 \leq x \leq \delta$ because over the interval $\delta \leq x \leq w/2$ the temperature differential is zero (i.e. $\theta(x,t) = 0$ for $\delta \leq x \leq w/2$ while $\delta < w/2$).

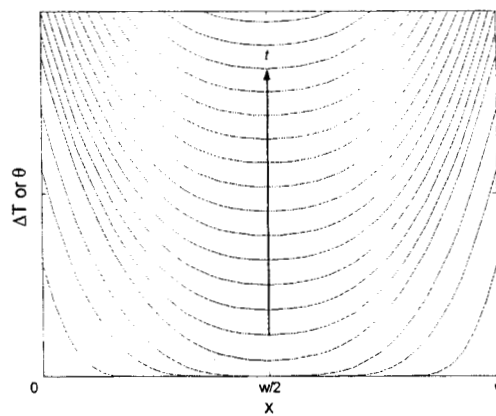


Figure 3. Dynamic temperature distribution in an infinite slab.

To approximate the average temperature of the rotor, the temperature distribution through the width of the rotor must be determined. The distribution at a radius sufficiently far away from the outer circumference can be approximated by treating the cross section of the rotor like an infinite slab with convection at both surfaces. It is assumed that both surfaces are exposed to the same fluid temperature. Thus the profile through the width will be symmetric about the centerline as shown in Figures

Figure 2 and Figure 3. Since the distribution is symmetric the half-slab case can be used (refer to

Figure 2 (b)) and the temperature can be averaged over half the width of the rotor. The boundary conditions then are,

$$\begin{aligned} \text{at } x = 0 & \quad \left(\frac{\partial \theta_{rotor}}{\partial x} \right)_{x=0} = \frac{h_r}{k_r} [\theta_{rotor}(0,t) - \theta_{compressor}(t)] \text{ and} \\ \text{at } x = w/2 & \quad \theta_{rotor}(\delta, t) = 0 \quad \left(\frac{\partial \theta_{rotor}}{\partial x} \right)_{x=w/2} = 0. \end{aligned}$$

Though the boundary conditions can be satisfied by using a quadratic distribution, significantly more accurate results are garnered by using the following cubic distribution [2],

$$\theta_{rotor}(x,t) = -\frac{h_r \delta(t)}{3k_r} [\theta_{rotor}(0,t) - \theta_{compressor}(t)] \left(1 - \frac{x}{\delta(t)} \right)^3. \quad (7)$$

By evaluating the above equation at $x = 0$ one can solve for $\theta(0,t)$,

$$\theta_{rotor}(0,t) = \frac{h_r \delta}{h_r \delta + 3k_r} \theta_{compressor}.$$

Substituting this into Equation (7) gives

$$\theta_{rotor}(x,t) = \frac{h_r \delta}{h_r \delta + 3k_r} \theta_{compressor} \left(1 - \frac{x}{\delta} \right)^3 \quad (8)$$

which has a partial derivative with respect to x of,

$$\frac{\partial \theta_{rotor}}{\partial x} = \frac{-3h_r}{h_r \delta + 3k_r} \theta_{compressor} \left(1 - \frac{x}{\delta} \right)^2. \quad (9)$$

The integral form of the conduction equation (Equation (6)) is used to calculate δ . Due to the boundary conditions, the second term on the left side and first term on the right of that equation are zero (i.e. $\theta_{rotor}(\delta, t) = 0$ and $(\partial \theta_{rotor} / \partial x)_{x=\delta} = 0$). Thus using the assumed temperature profile in Equation (8) and the temperature gradient in Equation (9), Equation (6) simplifies to

$$\frac{d}{dt} \left[\frac{h_r \delta}{h_r \delta + 3k_r} \theta_{compressor} \int_0^\delta \left(1 - \frac{x}{\delta} \right)^3 dx \right] - \theta_{rotor}(\delta, t) \frac{\partial x}{\partial t} = \alpha_r \left[\frac{3h_r}{h_r \delta + 3k_r} \theta_{compressor} \right]$$

which can be solved for δ ,

$$\delta = \left[\frac{12\alpha_r (h_r \delta + 3k_r)}{\theta_{compressor}} \int_0^\delta \frac{\theta_{compressor}}{h_r \delta + 3k_r} d\tau \right]^{1/2}. \quad (10)$$

Equations (7) and (10) can be used to simulate the dynamic temperature distribution up until the penetration depth reaches half the width of the rotor (i.e. while $\delta < w/2$). Once the penetration depth reaches half the width of the rotor (i.e. $\delta = w/2$), the thermal effects of the surface convection have penetrated fully and the temperature profile begins to rise. The half-slab temperature profile continues to be approximately cubic but now the distribution is

$$\theta_{rotor}(x,t) = [\theta_{rotor}(0,t) - \theta_{w/2}(t)] \left(1 - \frac{x}{w/2}\right)^3 + \theta_{w/2}(t) \quad (11)$$

where $\theta_{w/2}(t)$ is the centerline temperature differential which is zero until the penetration depth reaches the centerline. By evaluating the gradient of the assumed temperature profile at the surface and applying the convection boundary condition it can be shown that

$$\theta_{rotor}(0,t) = \frac{h_r(w/2)\theta_{compressor} + 3k_r\theta_{w/2}}{h_r(w/2) + 3k_r}$$

which when applied to Equation (11) gives the following temperature profile

$$\theta_{rotor}(x,t) = \frac{h_r(w/2)}{h_r(w/2) + 3k_r} (\theta_{compressor} - \theta_{w/2}) \left(1 - \frac{x}{w/2}\right)^3 + \theta_{w/2} \quad (12)$$

and thermal gradient

$$\frac{\partial}{\partial x} \theta_{rotor} = \frac{-3h_r}{h_r(w/2) + 3k_r} (\theta_{compressor} - \theta_{w/2}) \left(1 - \frac{x}{w/2}\right)^2 \quad (13)$$

By using Equations (6), (12), and (13) the rate change of centerline temperature can be calculated as

$$\dot{\theta}_{w/2} = \frac{1}{3h_r(w/2) + 12k_r} \left[-h_r(w/2)\dot{\theta}_{compressor} + \frac{12\alpha_r h_r}{w/2} (\theta_{compressor} - \theta_{w/2}) \right] \quad (14)$$

which can be integrated to determine the centerline temperature. Equations (12) and (14) can be used to simulate the half-slab temperature profile after the penetration depth reaches the centerline.

To summarize, the general equation for the approximate temperature distribution is

$$\theta_{rotor}(x,t) = \frac{h_r \delta}{h_r \delta + 3k_r} (\theta_{compressor} - \theta_{w/2}) \left(1 - \frac{x}{\delta}\right)^3 + \theta_{w/2} \quad (15)$$

where $\theta_{w/2} = 0$ for $\delta < w/2$. The penetration depth can be calculated using Equation (10) until it reaches the centerline at which point it remains constant and equal to half the rotor width. Thereafter, the centerline temperature is calculated using Equation (14). Equation (15) can be substituted into Equation (3) to calculate the width-wise average rotor temperature,

$$(\theta_{rotor})_{average} = \frac{h_r \delta \theta_{compressor} + (3h_r \delta + 12k_r) \theta_{w/2}}{4h_r \delta + 12k_r} \quad (16)$$

The rotor width will likely vary over the radius so the average width can be used to provide a reasonable approximation using the above equations.

2.2 Blades

As has already been mentioned for the turbine blades, the low ratio of volume to surface area suggests that the lumped-capacity method is applicable. More specifically, for most turbine blades the Biot number is small, $Bi = hL/k \ll 1$. Therefore, the approximate average blade temperature is

$$\dot{\theta}_{blade} = -\frac{h}{\rho c L} (\theta_{blade} - \theta_{ref}(t)) \tag{17}$$

where L is the characteristic length ($L = V / A$) and the reference temperature differential, θ_{ref} , is calculated using the film cooling effectiveness,

$$\eta = \frac{\theta_{ref} - \theta_{turbine}}{\theta_{compressor} - \theta_{turbine}} \tag{18}$$

(Note V and A are the blade volume and surface area.) As shown in Figure 4 the mainstream flow and film cooling flows have temperatures $T_{turbine}$ and $T_{compressor}$, respectively. Equations (17) and (18) are used to simulate the dynamic blade temperature.

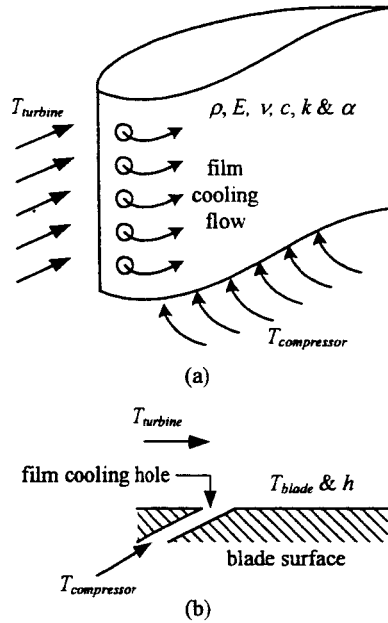


Figure 4. Blade schematic: (a) turbine blade and (b) blade surface.

2.3 Shroud/Casing

The shroud is a series of arcs circumferentially surrounding the turbine rotor and blades (refer to Figure 5). The arcs are mounted to the casing. Since the shroud is not one continuous rigid structure it is believed that the casing to which the shroud is attached dictates the radial deflection of the shroud. The inner surface of the casing is exposed to compressor discharge air. The outer surface conditions are questionable. To facilitate an approximation, it is assumed that turbine is mounted in a test rig where the outer casing surface is exposed to the atmosphere.

One could approximate the dynamic temperature distribution in the casing by using the cylindrical form of the conduction equation. However, this may unnecessarily complicate the solution because the wall thickness of the casing may be several orders of magnitude less than the radius of the casing (i.e. $(r_2 - r_1)/r_2 \ll 1$). Therefore, the casing can be approximated as a plane wall with two distinct boundary conditions as shown in Figure 6. This simplifies analysis and enables the use of a formulation similar to that used in §2.1. By using the principle of superposition, the two-boundary-condition problem can be broken in to two problems: (1) the temperature distribution due to thermal effects at the inner surface of the casing and (2) the temperature distribution due to the thermal effects at the outer surface of the casing (refer to Figure 6). One can calculate the temperature distributions due to convection at each surface and then sum the two solutions to approximate the overall distribution. Once the thermal effects of each side penetrate the width, the fully developed profile moves up the temperature axis as in Figure 7.

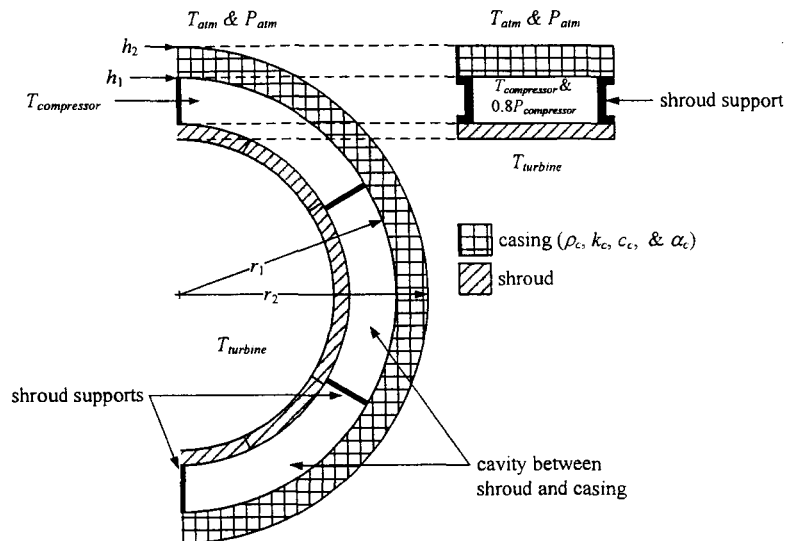


Figure 5. Shroud/casing schematic.

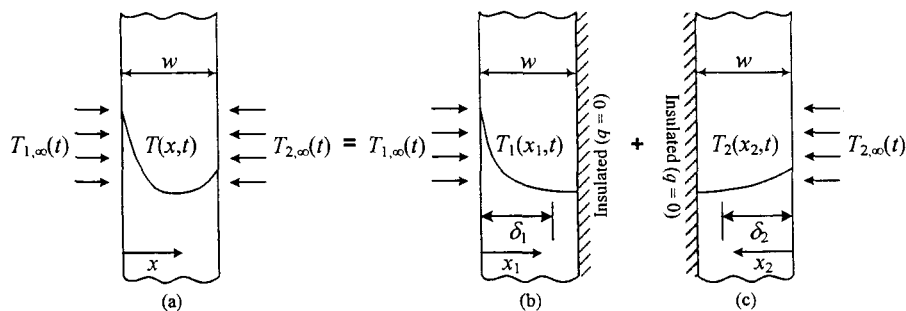


Figure 6. Infinite slab with two distinct boundary conditions: (a) temperature distribution, (b) distribution due to $T_{1,\infty}$ and (c) distribution due to $T_{2,\infty}$.

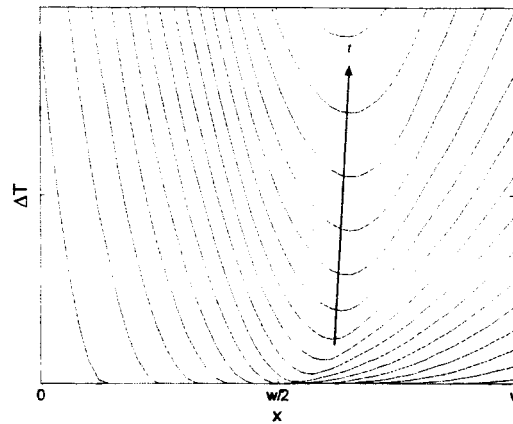


Figure 7. Temperature distribution in an infinite slab with two distinct convection boundary conditions.

Since the thickness of the casing is significantly less than the width of the rotor it is believed that a quadratic distribution (as opposed to a cubic distribution like that used for the rotor) should provide a sufficient approximation of the temperature distribution. The casing solution must be defined for the interval that the penetration depth is less than the casing thickness (i.e. $\delta < w$) and for the interval when it is equal to the casing thickness (i.e. $\delta = w$). To simplify derivation of each distribution, two coordinates are used: x_1 and x_2 . The first is measured from the inner surface edge and second from the outer surface edge. The two distributions can be easily summed by recognizing that $x_2 = w - x_1$. The temperature distributions can be derived in a similar fashion to the way the rotor distribution was.

By using a quadratic distribution and applying boundary conditions similar to those in Figure 6(b),

$$\begin{aligned} \text{at } x_1 = 0 \quad & \left(\frac{\partial}{\partial x} \theta_1 \right)_{x_1=0} = \frac{h_1}{k_c} [\theta_1(0, t) - \theta_{compressor}(t)] \text{ and} \\ \text{at } x_1 = w \quad & \theta_1(\delta_1, t) = 0 \quad \left(\frac{\partial}{\partial x} \theta_1 \right)_{x_1=w} = 0, \end{aligned}$$

it can be shown that the approximate temperature distribution due to the compressor discharge air is

$$\theta_1(x_1, t) = \frac{h_1 \delta_1}{h_1 \delta_1 + 2k_c} (\theta_{compressor} - \theta_{1,w}) \left(1 - \frac{x_1}{\delta_1} \right)^2 + \theta_{1,w} \quad (19)$$

where $\theta_{1,w}$, the outer surface temperature differential due to convection at the inner surface, is zero until the inner penetration depth reaches the outer surface (i.e. $\delta_1 = w$) at which point it is calculated using

$$\dot{\theta}_{1,w} = \frac{1}{2h_1 w + 6k_c} \left[-h_1 w \dot{\theta}_{compressor} + \frac{12\alpha_c h_1}{w} (\theta_{compressor} - \theta_{1,w}) \right] \quad (20)$$

which is derived using Equations (6) and (19). One can also use Equations (6) and (19) to derive the penetration depth due to thermal effects at the inner surface prior to reaching the outer surface,

$$\delta_1 = \left[\frac{6\alpha_c (h_1 \delta_1 + 3k_c)}{\theta_{compressor}} \int_0^{\theta_{compressor}} \frac{\theta_{compressor}}{h_1 \delta_1 + 3k_c} d\tau \right]^{1/2} \quad (21)$$

The component of the average temperature differential due to θ_1 is

$$(\theta_1)_{average} = \frac{h_1 \delta_1 \theta_{compressor} + (2h_1 \delta_1 + 6k_c) \theta_{1,w}}{3h_1 \delta_1 + 6k_c} \quad (22)$$

Similarly, one can determine the temperature distribution due to convection to atmosphere at the outer surface in terms of coordinate x_2 . Assuming for simplicity that the atmosphere is at a constant temperature, and that the boundary conditions are like those in Figure 6(c),

$$\begin{aligned} \text{at } x_2 = 0 & \quad \left(\frac{\partial \theta_2}{\partial x} \right)_{x_2=0} = \frac{h_2}{k_c} [\theta_2(0,t) - \theta_{atm}] \text{ and} \\ \text{at } x_2 = w & \quad \theta_2(\delta_2, t) = 0 \quad \left(\frac{\partial \theta_2}{\partial x} \right)_{x_2=w} = 0, \end{aligned}$$

the temperature distribution due to the thermal effects at the outer surface is

$$\theta_2(x_2, t) = \frac{h_2 w}{h_2 w + 2k_c} (\theta_{atm} - \theta_{2,w}) \left(1 - \frac{x_2}{w} \right)^2 + \theta_{2,w} \quad (23)$$

where $\theta_{2,w}$, the inner surface temperature differential due to convection at the outer surface, is zero until the outer penetration depth reaches the inner surface (i.e. $\delta_2 = w$), and then it is calculated from

$$\dot{\theta}_{2,w} = \frac{3\alpha_c h_2}{w(h_2 w + 3k_c)} (\theta_{atm} - \theta_{2,w}) \quad (24)$$

which is also derived using the integral form of the conduction equation. The component of the average temperature due to θ_2 is

$$(\theta_2)_{average} = \frac{h_2 \delta_2 \theta_{atm} + (2h_2 \delta_2 + 6k_c) \theta_{2,w}}{3h_2 \delta_2 + 6k_c} \quad (25)$$

The overall average temperature can be approximated by summing Equations (22) and (25).

3 Results

Based on results for a validated model, it was determined that the previous turbine tip clearance model erroneously estimated the temperatures for the shroud/casing, blades, and rotor. As shown in Figure 8 the commercial model (---CES) estimated a slower transient for the rotor and a more pronounced transient for the blade relative to the original turbine tip clearance model (—ACC).

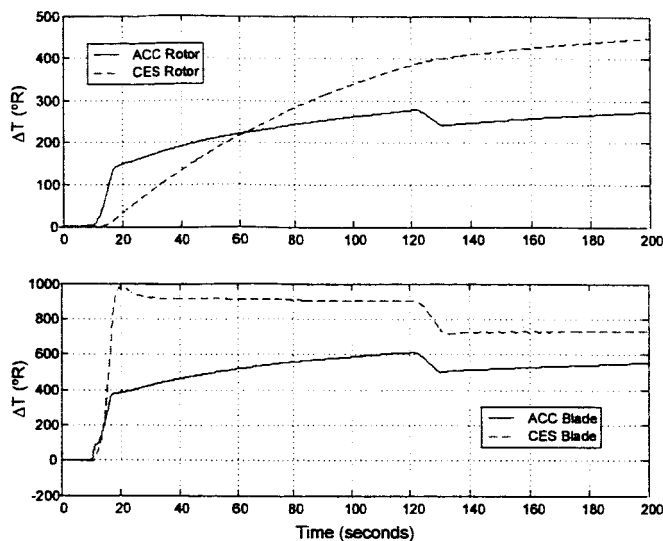


Figure 8. Comparison of original model (ACC) to validated results (CES).

By implementing the corrections detailed in §2.1 and §2.2 the new simulation produces the results in Figure 9. Note how the new results (—ACC2) for the rotor almost exactly match the CES estimation. The blade results are also much improved over the previous model. Furthermore, as was detailed in [1] many of the parameters were estimated based on numbers found in literature, and with minor adjustments or improvements to the values used, the new model can match the CES model more closely.

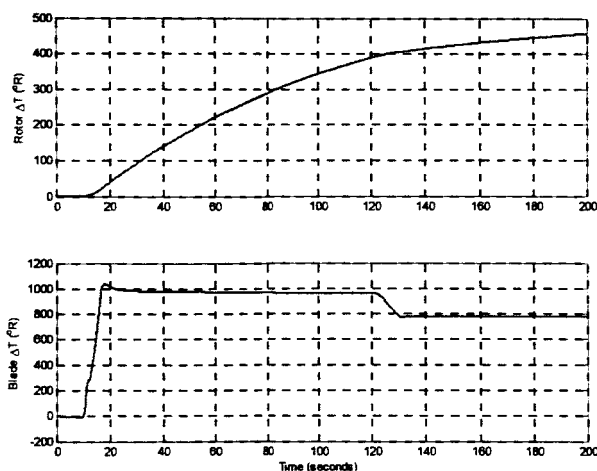


Figure 9. Temperature estimations using approximations detailed in §2.1 and §2.2.

Figure 10 shows the average temperature estimation for the casing using the analysis from §2.3. The results are similar in form to the estimation for the rotor.

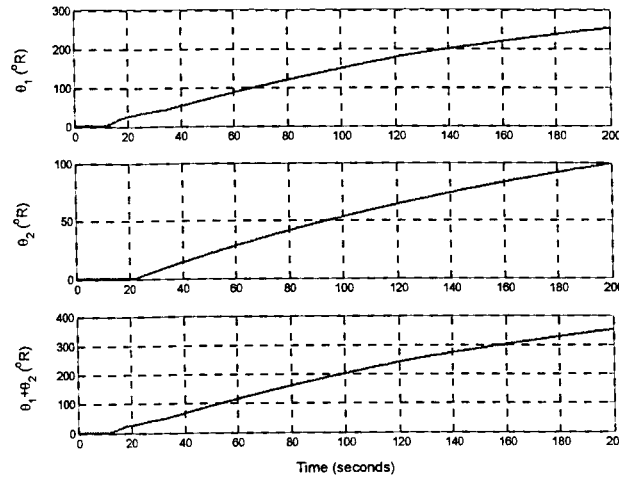


Figure 10. Temperature estimation for casing using approximation in §2.3.

4 Discussion

As was expected, some of the assumptions used in the original model were inappropriate, particularly assumptions 3 and 4. Assumption 5 appears to be reasonable because the improved results detailed above were achieved without incorporating temperature-dependent material properties. However, one should note that the approximate method used for the rotor and casing can be adapted to incorporate material property temperature dependencies. By using a transformation suggested by Goodman [4],

$$v(x,t) = \int_0^{\theta} \rho c d\theta ,$$

in the conduction equation (Equation (4)), one will yield

$$\frac{\partial v}{\partial t} = \frac{\partial}{\partial x} \left[\alpha(v) \frac{\partial v}{\partial x} \right]$$

which can be integrated with respect to x for an equivalent integral form of the conduction equation,

$$\frac{d}{dt} \left[\int_0^{\delta} v dx \right] - v(\delta,t) \frac{d\delta}{dt} = -\alpha(v(0,t)) \frac{\partial v}{\partial x} \Big|_{x=\delta} .$$

By using the approximate method of assumed solutions, a estimation incorporating temperature dependencies could be derived with some work, but based on the current results the added effort would likely be unnecessary.

In conclusion, the improved estimations provided herein would substantially advance the existing model while maintaining the relative simplicity desired to facilitate design of the future active clearance control.

References

1. Kypuros, J. A. and Melcher, K. J., "A Reduced Model for Estimation of Thermal and Rotational Effects on Turbine Tip Clearance," NASA TM-2003-212226, 2003.

2. Eckert, E. R. G. and Drake Jr., R. M., *Analysis of Heat and Mass Transfer*, Hemisphere Publishing Corporation, New York, NY, 1987.
3. Gebhart, B., *Heat Conduction and Mass Diffusion*, McGraw-Hill, Inc., New York, NY, 1993.
4. Goodman, T. R., "The Heat Balance Integral and Its Application to Problems Involving a Change in Phase", *Transaction of the ASME*, **8**(2), 1958.
5. Goodman, T. R., "The Heating of Slabs with Arbitrary Heat Inputs", *Journal of Aerospace Science*, **26**(187), 1959.